

Dominant phonon wave vectors and strain-induced splitting of the 2D Raman mode of graphene

Rohit Narula,^{1,2,*} Nicola Bonini,³ Nicola Marzari,³ and Stephanie Reich²

¹*Department of Materials Science and Engineering, Massachusetts Institute of Technology, Cambridge, Massachusetts 02139, USA*

²*Fachbereich Physik, Freie Universität Berlin, Arnimallee 14, 14195 Berlin, Germany*

³*Department of Materials, University of Oxford, Oxford OX1 3PH, United Kingdom*

(Received 25 February 2011; revised manuscript received 2 February 2012; published 30 March 2012)

The dominant phonon wave vectors \mathbf{q}^* probed by the 2D Raman mode of pristine and uniaxially strained graphene are determined via a combination of *ab initio* calculations and a full two-dimensional integration of the transition matrix. We show that \mathbf{q}^* are highly anisotropic and rotate about \mathbf{K} with the polarizer and analyzer condition relative to the lattice. The corresponding phonon-mediated electronic transitions show a finite component along $\mathbf{K}-\Gamma$ that sensitively determines \mathbf{q}^* . We invalidate the notion of “inner” and “outer” processes. The characteristic splitting of the 2D mode of graphene under uniaxial tensile strain and given polarizer and analyzer setting is correctly predicted only if the strain-induced distortion and red-shift of the in-plane transverse optical (iTO) phonon dispersion as well as the changes in the electronic band structure are taken into account.

DOI: [10.1103/PhysRevB.85.115451](https://doi.org/10.1103/PhysRevB.85.115451)

PACS number(s): 81.05.ue, 63.22.Rc, 78.67.Wj

Graphene¹ is actively researched both for its fundamental physics and technological applications.² The high mobility of its charge carriers even at high-bias-induced concentrations¹ endows it with ballistic conduction at room temperature, making graphene a promising material for both transistors and interconnects. It is also emerging as an ultrasensitive probe for measuring strain.³ Such properties are essentially mediated by phonons. For instance, the high-bias current transport is limited by scattering with optical phonons,⁴ while the response to deformation is linked to the vibrational properties through the Grüneisen parameters.³ More fundamentally, quasiparticle lifetimes in graphene are determined in part by electron-phonon coupling involving optical phonons.⁵ An accurate experimental determination of the two-dimensional phonon dispersion $\omega(\mathbf{q})$ of graphene is thus critical.

Raman spectroscopy can accurately measure phonons in graphene, yielding information on the number of graphene layers,⁶ lattice orientation,^{3,7} doping,⁸ disorder,⁹ edge structure,¹⁰ and phonon anharmonicities.¹¹ The unique electronic band structure of graphene¹² provides the prominent 2D Raman feature at $\sim 2700\text{ cm}^{-1}$ for visible irradiation that probes the in-plane transverse optical (iTO) branch of the phonon dispersion with wave vectors $\mathbf{q} \sim \mathbf{K}$.^{6,13} This dispersive mode stems from a second-order Raman process involving intervalley ($\mathbf{K} \rightarrow \mathbf{K}'$) scattering of the electron and hole quasiparticles.¹⁴

With the notable exception of the analytical work by Basko¹⁵ treating the idealized case of Dirac cones, studies of the 2D mode^{16–18} are often based on the simplification that the dominant phonon wave vectors \mathbf{q}^* and the associated phonon-mediated electronic transitions are fixed regardless of the polarization of light in the Raman experiment. Moreover, the electronic transitions are deemed to occur along the high-symmetry $\mathbf{K}-\mathbf{M}-\mathbf{K}'$ direction. By definition they are labeled inner^{17,19,20} and outer^{6,16,19} transitions depending on whether they connect the closer or further parts, respectively, of the equiexcitation energy contours of the electronic dispersion centered at \mathbf{K} and \mathbf{K}' and across the \mathbf{M} point. These *ad hoc* notions are based on two assumptions. The first is that the

electronic bands around \mathbf{K} are one-dimensional and linear, thus failing to capture their electron-hole asymmetry and the trigonal warpings of both the electronic and phonon bands that become prominent at visible laser frequencies.^{21–23} Reducing the two-dimensional Brillouin zone (BZ) of graphene into a single dimension also misses the effects of quantum mechanical interference.^{17,24} The second assumption is that the electronic and phonon wave-vector dependence of the optical matrix elements and the electron-phonon matrix elements in the scattering process^{14,17,24} are negligible despite their highly anisotropic profiles.^{4,25}

In this article we determine the dominant iTO phonon wave vectors \mathbf{q}^* and the associated dominant phonon-mediated electronic transitions probed by the 2D Raman mode of graphene. We consider pristine graphene and graphene subject to uniaxial tensile strains up to 2%. We explicitly include the variation of the matrix elements together with the two-dimensional electronic and phonon bands obtained from *ab initio* calculations, employing them in a full two-dimensional integration of the transition matrix. The \mathbf{q}^* obtained from our calculations are highly anisotropic and rotate about \mathbf{K} with the polarizer and analyzer condition relative to the crystallographic orientation of graphene. The associated dominant phonon-mediated electronic transitions are neither fixed nor parallel to the $\mathbf{K}-\mathbf{M}-\mathbf{K}'$ direction, but show a component along $\mathbf{K}-\Gamma$. We further show that the strain-induced splitting of the 2D mode requires consideration of the distortion and red-shift of the iTO phonon band and changes in the resonance condition, the latter of which was hinted at previously.^{18,20}

The transition matrix $\mathcal{T}_{fi}(\mathbf{q})$ corresponding to the 2D mode in graphene, containing the leading terms²⁶ from fourth-order perturbation theory, is evaluated with a single broadening parameter $\gamma = 0.05\text{ eV}$ and a full two-dimensional integration over the graphene BZ.²⁷ The electronic eigenfunctions and the optical matrix elements are computed using density functional theory (DFT) within the local density approximation (LDA). The iTO phonon branch and the electron-phonon matrix elements are calculated using density functional perturbation theory (DFPT).²⁸ All calculations are performed using the

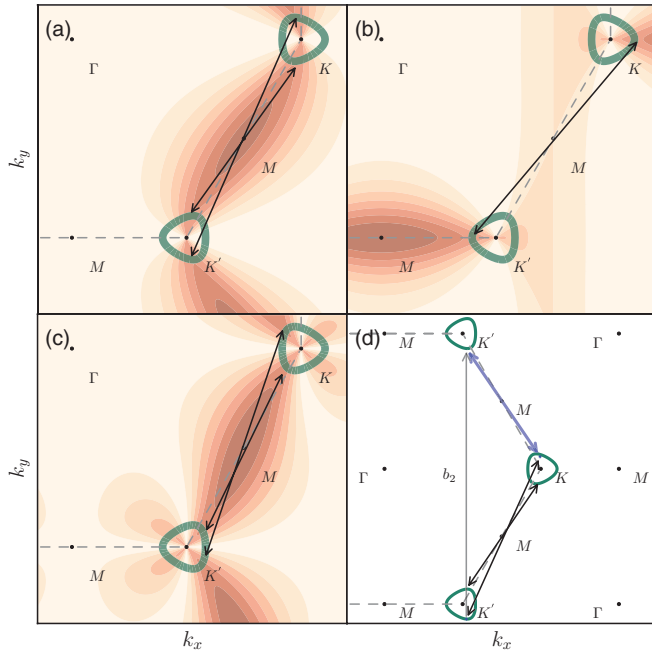


FIG. 1. (Color online) The phonon-mediated electronic transitions yielding maximum intensity (black double-sided arrows) contributing to the 2D mode. These transitions were extracted from a full integration of the transition matrix. The underlying yellow-red contour plots of panels (a)–(c) are the product of the optical absorption and emission matrix elements at the polarizer and analyzer orientations (a) $x : x$, (b) $y : y$, and (c) $x : y$ (x , zigzag; y , armchair orientation of graphene), respectively. The equiexcitation energy contours corresponding to the laser energy are represented by green lines. (d) For the $x : x$ case, on adding a reciprocal lattice vector \mathbf{b}_2 to \mathbf{k}_i^* , from the seemingly outer dominant transition (black double-sided arrow connecting the black crosshairs) an equivalent inner electronic transition (blue double-sided arrow) is obtained.

Quantum ESPRESSO²⁹ distribution and the parameters of the simulations taken from Ref. 11. For unstrained graphene we correct the LDA eigenenergies with the results of recent GW calculations. In particular, we use two-dimensional GW -derived electronic bands³⁰ fit to a third-nearest-neighbor tight-binding description²¹ and a fit proposed in Ref. 22 for the iTO phonon dispersion around \mathbf{K} . The dominant electronic transitions connecting the initial \mathbf{k}_i^* and final \mathbf{k}_f^* electron wave vectors are determined from the arguments of $\text{Max}[|\mathcal{T}_{fi}(\mathbf{k}_i, \mathbf{q})|^2]$ and the relation expressing quasimomentum conservation during the phonon-assisted scattering of the electron ($\mathbf{k}_i^* = \mathbf{k}_f^* + \mathbf{q}^*$).

The phonon-mediated electronic transitions yielding the highest intensity for polarizer and analyzer combinations $x : x$, $y : y$, and $x : y$ (x , zigzag; y , armchair orientation of graphene) are shown in Fig. 1. The resonant transitions connect equiexcitation energy contours where the product of the optical matrix elements is strongest. Interestingly, they are not qualitatively affected by the electron-phonon matrix elements. Although the structure of the optical matrix elements' product enforces the preponderant phonon-assisted transitions to lie nominally along the $\mathbf{K}-\mathbf{M}-\mathbf{K}'$ line, the small component in the $\mathbf{K}-\Gamma$ direction sensitively determines the angular location of \mathbf{q}^* [see the blue-green regions of Figs. 2(a)–2(c)]. Consequently,

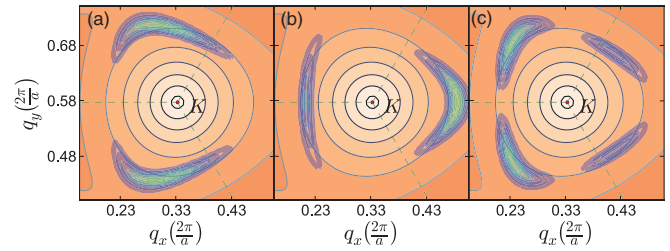


FIG. 2. (Color online) The dominant phonon wave vectors \mathbf{q}^* (in blue-green) corresponding to polarizer and analyzer orientations: (a) $x : x$, (b) $y : y$, and (c) $x : y$. The underlying orange-hued contours depict the iTO phonon dispersion of Ref. 22 around \mathbf{K} .

\mathbf{q}^* are highly anisotropic, rotate about \mathbf{K} with different polarizer and analyzer combinations, and are not, in general, restricted along high-symmetry lines. Further, by translating \mathbf{k}_i^* by a reciprocal lattice vector \mathbf{b}_2 , the character of the dominant phonon-mediated electronic transition changes from being seemingly outer, as defined, to an equivalent inner transition [see Fig. 1(d)], undermining the distinction between them. We thus revoke the notion of fixed inner and outer electronic transitions parallel to the high-symmetry $\mathbf{K}-\mathbf{M}-\mathbf{K}'$ direction.

Free from external, symmetry-breaking potentials, graphene is characterized by a nominally single 2D Raman mode peak for visible irradiation.⁶ The apparent anisotropy of \mathbf{q}^* notwithstanding, \mathbf{q}^* closely follow the trigonal phonon equifrequency contours [see Figs. 2(a)–2(c)]. However, with the application of uniaxial tensile strain, experiments show that the 2D mode of graphene broadens and then splits while shifting to lower wave numbers.^{18,31} The characteristic peak shape and magnitude of the effects depend on the polarizer and analyzer condition and strain direction relative to the lattice as well as the laser energy. In Refs. 18,19, and 32 the splitting of the 2D mode under uniaxial tensile strain was attributed primarily to the shift of the Dirac cones from \mathbf{K} .³³ References 18 and 20 additionally implicated the inner process along the $\mathbf{K}-\mathbf{M}$ direction as dominant; the iTO phonon dispersion was assumed to be symmetric¹⁸ or “more or less” symmetric²⁰ around \mathbf{K} while allowing for phonon softening.

An LDA + DFPT calculation³⁴ for graphene subject to uniaxial tensile strains up to 2% along the zigzag and armchair orientations reveals phonon softening and, crucially, the distortion of trigonal warping of the two-dimensional phonon dispersion. This is apparent when comparing the undistorted phonon equifrequency contours of Fig. 2 with those of graphene strained along the zigzag [Fig. 4(g)] and armchair directions [Fig. 4(i)]. We also observe a shift of the Kohn anomaly³⁵ away from \mathbf{K} as expected.³³ For fixed laser energy, increasing the tensile strain results in a red-shift of the calculated 2D mode as shown in Fig. 3 with concomitant broadening and eventual splitting of the 2D peak in agreement with experiment.^{18,19,32} We note that there is currently a disagreement in the literature^{3,7} regarding the strain rates of the G^- and G^+ Raman modes used to calibrate strain; Huang *et al.*^{7,18} estimate strain levels a factor of three higher than Mohiuddin *et al.*³ and our own *ab initio* results: $\frac{\partial \omega_{G^-}}{\partial \varepsilon} = -34 \text{ cm}^{-1}/\%$ and $\frac{\partial \omega_{G^+}}{\partial \varepsilon} = -15 \text{ cm}^{-1}/\%$. Recent measurements in the infrared region of Ref. 31 are

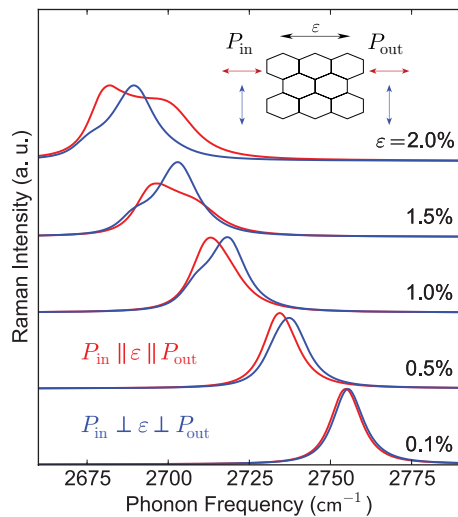


FIG. 3. (Color online) 2D Raman mode spectra calculated for increasing strain along the zigzag direction of graphene. Compare with Fig. 1(a) of Ref. 18. The inset highlights the orientation of graphene relative to strain and the polarization of incoming and outgoing light.

consistent with those of Ref. 3 and therefore we compare with the measurements of Huang *et al.*^{7,18} at a strain that is approximately one-third of theirs.

We now compare the relative position between the calculated 2D modes for graphene as a function of uniaxial strain ϵ along the zigzag direction to experiment [compare with Fig. 1(a) of Ref. 18] for incoming light polarization $P_{in} \parallel \epsilon$ (red lines in Fig. 3) and $P_{in} \perp \epsilon$ (blue lines in Fig. 3).³⁶ The dominant peak for $P_{in} \parallel \epsilon$ is red-shifted compared to that for $P_{in} \perp \epsilon$, while the subdominant peaks are blue- and red-shifted to their respective dominant peaks, consistent with the measurements of Huang *et al.*¹⁸

Figures 4(a)–4(c) exhibit the experimental data for various strains and polarizer and analyzer combinations employed by Huang *et al.*¹⁸ The data are compared to our calculations in Figs. 4(d)–4(f). Our first-principles calculations combined with fourth-order perturbation theory successfully reproduce the characteristic two-peak behavior and the correct polarization dependence of the 2D mode under strain. For example, the calculate 2D mode for ϵ oriented along the zigzag direction and $P_{in} \parallel \epsilon$ and $\psi = 0^\circ$ [black curve of Fig. 4(e)] possesses a red-shifted subdominant peak consistent with experiment [black curve of Fig. 4(b)]. For strain along the armchair direction and $P_{in} \perp \epsilon$ and $\psi = 0^\circ$ [black curve of Fig. 4(f)] we achieve a nearly symmetric peak as obtained experimentally [black curve of Fig. 4(c)]. We note that our calculations consistently overestimate the relative intensity of the side bands and our spectra are blue-shifted in comparison to experiment. The origin of both these discrepancies between our parameter-free calculations and experiment lies in the tendency of the LDA functional to underestimate the slopes of both the electronic³⁰ and iTO phonon bands³⁷ of graphene around \mathbf{K} . The absolute position and integrated intensities of the 2D mode are highly sensitive to the Fermi velocity and iTO phonon band slope, a fact supported by our calculations and an analytical model.¹⁵ Overall, given the complexity of both our *ab initio* and

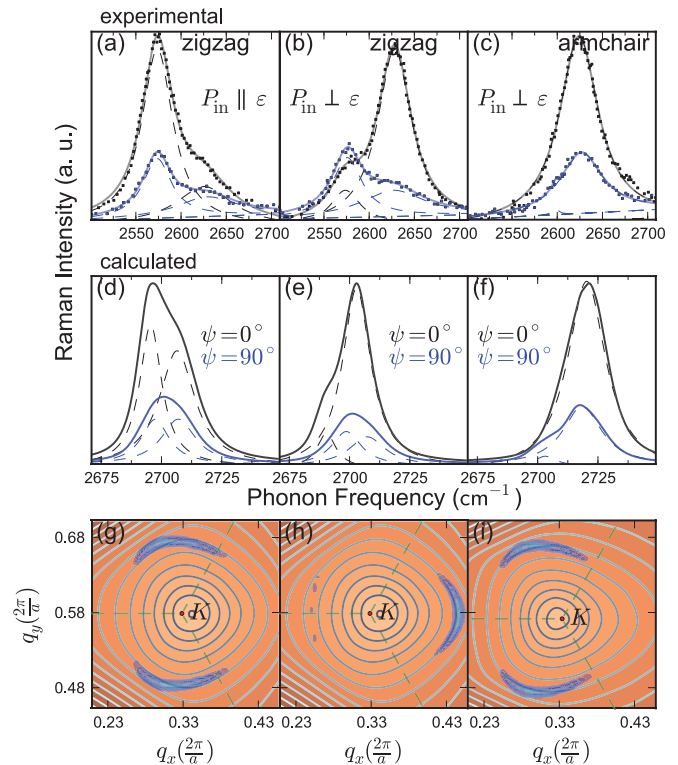


FIG. 4. (Color online) Experimental¹⁸ [panels (a)–(c) (dotted points)] and calculated [panels (d)–(f) (solid lines)] polarized 2D Raman spectra for incoming polarization P_{in} and outgoing polarization ψ relative to P_{in} . Panels (a) and (d) and panels (b) and (e): Zigzag direction of strain. Panels (c) and (f): Armchair directions of strain. The dashed lines represent Lorentzian fits to the spectra. Panels (g)–(i): The orange-hued contours depict the iTO phonon dispersion and the blue-green regions are \mathbf{q}^* for graphene subject to $\epsilon = 1.5\%$ along the zigzag direction [panels (g) and (h)] and $\epsilon = 1.0\%$ along the armchair direction (i).

fourth-order theory calculations and the 2D Raman mode measurements under strain, our results capture very well the key spectroscopic features observed in the experiment and, more interestingly, provide a clear insight into their microscopic origin.

The distinctive splitting of the 2D mode under uniaxial strain and varying polarizer and analyzer orientation arises from strain-induced changes in the electronic and phonon bands. It cannot be explained by the movement of the Dirac cones alone.¹⁸ For example, for strain along the zigzag direction and $P_{in} \parallel \epsilon \parallel P_{out}$, a combination of strained electronic bands and an unstrained phonon dispersion [Fig. 5(b)] produces a symmetric peak. In contrast, the full calculation considering the strained versions of both the electronic and phonon dispersions predicts [Fig. 5(a)] a shoulder above the frequency of the main peak as seen experimentally [Fig. 4(a)]. A calculation including the strained phonon dispersion and unstrained electronic bands [Fig. 5(c)] also successfully reproduces the relative positions of the two peaks seen in the experiment. However, for armchair strain and $P_{in} \perp \epsilon \perp P_{out}$ (not shown), subjecting only the phonon dispersion to strain results in a blue-shifted side peak. This contradicts the experimentally obtained symmetric peak of

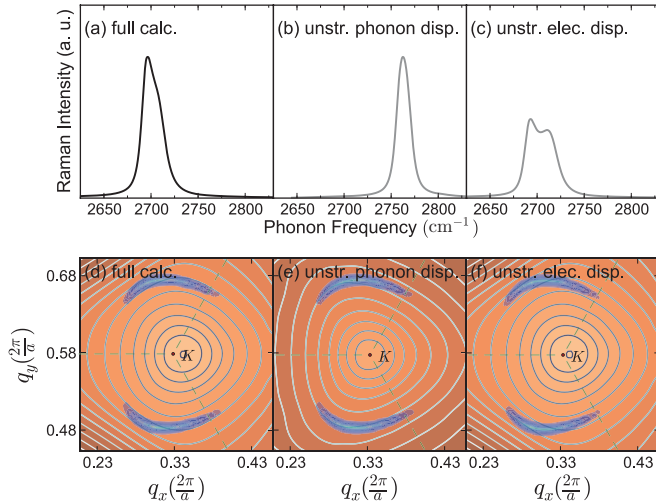


FIG. 5. (Color online) 2D Raman mode spectra obtained from (a) a full calculation considering the strained phonon and electronic bands for the zigzag orientation having $P_{in} \parallel \varepsilon \parallel P_{out}$ [compare with Fig. 4(a)]. (b) Calculation using an unstrained phonon dispersion plus strained electronic bands as input for the transition matrix calculation. (c) Calculation using a strained phonon dispersion and unstrained electronic bands. The corresponding orange-hued iTO phonon contours and blue-green regions for \mathbf{q}^* are given in panels (d)–(f).

Fig. 4(c). These observations show that the distortion of the iTO phonon dispersion, the phonon softening, and changes in the electronic structure under strain are indispensable for correctly reproducing the characteristic splitting of the 2D mode.

In summary, by including the two-dimensional electronic bands, iTO phonon dispersion, and matrix elements in a full two-dimensional integration of the transition matrix, we show that the \mathbf{q}^* of the 2D Raman mode of graphene display a highly anisotropic structure and rotate about \mathbf{K} with the polarizer and analyzer setting with respect to the crystallographic orientation

of graphene. The associated dominant phonon-mediated electronic transitions are neither fixed nor parallel to the $\mathbf{K}-\mathbf{M}-\mathbf{K}'$ direction. Instead, a small but significant contribution of the $\mathbf{K}-\mathbf{\Gamma}$ direction is discerned, connecting regions where the product of the optical absorption and emission matrix elements is strongest. Furthermore, the phonon-mediated transitions can be transformed with the addition of a reciprocal lattice vector into each other, thereby dismissing the notion of inner and outer processes. Our analysis, when applied to the 2D mode for graphene subject to a range of uniaxial tensile strains demonstrates that its characteristic splitting with specific polarizer and analyzer combinations and strain orientation is only reproducible by consideration of the strained versions of both the electronic bands and the iTO phonon band. Since the theoretical description of the 2D mode is closely related to the defect-activated D mode,¹³ we expect our results to hold for the D mode as well.

Recently we became aware of a theoretical work by Venezuela *et al.*³⁸ investigating the Raman 2D mode in graphene via *ab initio* calculations. While they find that the phonons probed by the 2D mode “belong to limited regions of the BZ consisting in very narrow (almost one-dimensional) lines” and “The most important phonons belong to the $\mathbf{K}-\mathbf{\Gamma}$ direction (inner phonons) and not to the $\mathbf{K}-\mathbf{M}$ one (outer phonons) ...” for the particular case of unpolarized input light and detection,³⁹ our results for the case of linear polarizer and analyzer combinations emphasize that their conclusion is not general. Instead, the angular location of the dominant phonon wave vectors \mathbf{q}^* around \mathbf{K} is determined by the polarization conditions [see for instance Fig. 2(b) where the $\mathbf{K}-\mathbf{M}$ contribution is clearly present], a fact confirmed by the successful reproduction of polarized 2D Raman mode spectra of graphene under uniaxial strain as shown above.

This work was supported by the MIT Institute of Soldier Nanotechnologies (ISN) and the European Research Council (ERC) under Grant No. 210642-OptNano.

*rnarula@mit.edu

¹K. S. Novoselov *et al.*, *Science* **306**, 666 (2004).
²A. K. Geim and K. S. Novoselov, *Nat. Mater.* **6**, 183 (2007).
³T. M. G. Mohiuddin *et al.*, *Phys. Rev. B* **79**, 205433 (2009).
⁴S. Piscanec, M. Lazzeri, F. Mauri, A. C. Ferrari, and J. Robertson, *Phys. Rev. Lett.* **93**, 185503 (2004).
⁵C.-H. Park, F. Giustino, C. D. Spataru, M. L. Cohen, and S. G. Louie, *Phys. Rev. Lett.* **102**, 076803 (2009).
⁶A. C. Ferrari *et al.*, *Phys. Rev. Lett.* **97**, 187401 (2006).
⁷M. Huang *et al.*, *Proc. Natl. Acad. Sci. USA* **106**, 7304 (2009).
⁸S. Pisana *et al.*, *Nat. Mater.* **6**, 198 (2007).
⁹A. C. Ferrari, *Solid State Commun.* **143**, 47 (2007).
¹⁰L. G. Cançado, M. A. Pimenta, B. R. A. Neves, M. S. S. Dantas, and A. Jorio, *Phys. Rev. Lett.* **93**, 247401 (2004).
¹¹N. Bonini, M. Lazzeri, N. Marzari, and F. Mauri, *Phys. Rev. Lett.* **99**, 176802 (2007).

¹²P. R. Wallace, *Phys. Rev.* **71**, 622 (1947).
¹³S. Reich and C. Thomsen, *Philos. Trans. R. Soc. A* **362**, 2271 (2004).
¹⁴C. Thomsen and S. Reich, *Phys. Rev. Lett.* **85**, 5214 (2000).
¹⁵D. M. Basko, *Phys. Rev. B* **78**, 125418 (2008).
¹⁶R. Saito, A. Jorio, A. G. Souza Filho, G. Dresselhaus, M. S. Dresselhaus, and M. A. Pimenta, *Phys. Rev. Lett.* **88**, 027401 (2001).
¹⁷J. Maultzsch, S. Reich, and C. Thomsen, *Phys. Rev. B* **70**, 155403 (2004).
¹⁸M. Huang *et al.*, *Nano Lett.* **10**, 4074 (2010).
¹⁹M. Mohr, J. Maultzsch, and C. Thomsen, *Phys. Rev. B* **82**, 201409 (2010).
²⁰D. Yoon, Y.-W. Son, and H. Cheong, *Phys. Rev. Lett.* **106**, 155502 (2011).

- ²¹S. Reich, J. Maultzsch, C. Thomsen, and P. Ordejón, *Phys. Rev. B* **66**, 035412 (2002).
- ²²A. Gruneis *et al.*, *Phys. Rev. B* **80**, 085423 (2009).
- ²³R. Narula, R. Panknin, and S. Reich, *Phys. Rev. B* **82**, 045418 (2010).
- ²⁴R. Narula and S. Reich, *Phys. Rev. B* **78**, 165422 (2008).
- ²⁵A. Gruneis, R. Saito, G. G. Samsonidze, T. Kimura, M. A. Pimenta, A. Jorio, A. G. Souza Filho, G. Dresselhaus, and M. S. Dresselhaus, *Phys. Rev. B* **67**, 165402 (2003).
- ²⁶The leading terms are composed of four Feynman diagrams, each with a light-matter interaction vertex at both ends. In between, the first two contain an electron-phonon interaction vertex on both the electron and the hole channels⁴⁰ that when interchanged enumerates the two time orders. The remaining two, subordinate contributions contain both the electron-phonon interaction vertices on either the electron or the hole channel, separately.¹⁴
- ²⁷R. Narula, Ph.D. thesis, Massachusetts Institute of Technology, 2011.
- ²⁸S. Baroni, S. de Gironcoli, A. Dal Corso, and P. Giannozzi, *Rev. Mod. Phys.* **73**, 515 (2001).
- ²⁹P. Giannozzi *et al.*, *J. Phys.: Condens. Matter* **21**, 395502 (2009).
- ³⁰A. Gruneis, C. Attaccalite, L. Wirtz, H. Shiozawa, R. Saito, T. Pichler, and A. Rubio, *Phys. Rev. B* **78**, 205425 (2008).
- ³¹O. Frank *et al.*, *ACS Nano* **5**, 2231 (2011).
- ³²M. Mohr, K. Papagelis, J. Maultzsch, and C. Thomsen, *Phys. Rev. B* **80**, 205410 (2009).
- ³³V. M. Pereira, A. H. Castro Neto, and N. M. R. Peres, *Phys. Rev. B* **80**, 045401 (2009).
- ³⁴Our calculations were performed at a laser energy (1.5 eV) lower than that of experiment (2.3 eV), necessitated in order to obtain reasonable magnitudes of the relevant electronic and phonon wave vectors as expected by more accurate functionals than LDA.
- ³⁵W. Kohn, *Phys. Rev. Lett.* **2**, 393 (1959).
- ³⁶Since the outgoing polarization P_{out} was not discerned in Ref. 18, we chose to set it parallel to the incoming one, maximizing the integrated intensity of the 2D mode.
- ³⁷M. Lazzeri, C. Attaccalite, L. Wirtz, and F. Mauri, *Phys. Rev. B* **78**, 081406 (2008).
- ³⁸P. Venezuela, M. Lazzeri, and F. Mauri, *Phys. Rev. B* **84**, 035433 (2011).
- ³⁹It is worth noting that in practice the internal optics of Raman spectrometers have a preferred polarization direction where their response is maximized, effectively yielding *polarized* Raman measurements.
- ⁴⁰R. Loudon, *Adv. Phys.* **13**, 423 (1964).